

Future Change of Tornadogenesis-Favorable Environmental Conditions in Japan Estimated by a 20-km-Mesh Atmospheric General Circulation Model

Takanari MURAMATSU

Hakodate Airport Branch, Hakodate, Japan

Teruyuki KATO

Meteorological Research Institute, Tsukuba, Japan

Masahisa NAKAZATO

Japan Meteorological Agency, Chiyoda, Japan

Hirokazu ENDO

Meteorological Research Institute, Tsukuba, Japan

and

Akio KITO

Faculty of Life and Environmental Sciences, University of Tsukuba, Tsukuba, Japan

(Manuscript received 30 October 2014, in final form 24 August 2015)

Abstract

Because tornadoes cause enormous damage to humans and societies, projecting plausible future changes in tornado activity is an important research focus. We used the results of climate experiments under the A1B emissions scenario with a 20-km-mesh and a high-resolution atmospheric global circulation model to project future changes in the frequency of conditions conducive to the generation of strong tornadoes (F2 or greater on the Fujita scale) in Japan. We found that this frequency is likely to double in future in almost all areas of the Japanese Islands in spring and on the Japan Sea side of the Japanese Islands in summer due to intensification of atmospheric instability caused by an increase in the water-vapor mixing ratio and a temperature rise in the lower troposphere. In contrast, the frequency of strong vertical wind shear, which is conducive to tornadogenesis, was projected to hardly change or decrease slightly. Comparison with climate fields generated by a 60-km-mesh 12-member ensemble experiment showed that future changes in tornadogenesis-favorable environmental conditions projected by the 20-km-mesh experiment were highly reliable. Moreover, we found that the predicted future changes were robust when we used other thresholds for the environmental parameters that created conditions conducive to strong tornadoes. Our results indicate that there will be a significant increase in the frequency of strong tornadoes in Japan in the future.

Keywords tornado; global warming; general circulation model (GCM)

Corresponding author: Takanari Muramatsu, Hakodate Airport Branch, Japan Meteorological Agency, 511 Takamatsu-cho, Hakodate, Hokkaido 042-0952, Japan
E-mail: takanari_muramatsu@met.kishou.go.jp
©2016, Meteorological Society of Japan

1. Introduction

Tornadoes cannot be directly simulated by current climate models because the typical scales of tornadoes (horizontal spatial and time scales are approximately 100 m and 10 min, respectively) are far smaller than the resolution of climate models. In contrast, the occurrence probability of a parent cloud system causing strong tornadoes (i.e., a supercell storm) can be estimated from upper air soundings related to convective instability and vertical wind shear (Rasmussen and Blanchard 1998; Thompson et al. 2003). Strong tornadoes occur in atmospheric environmental fields with significant convective instability and adequate vertical wind shear. Several studies have projected an increase in the frequency of severe storms that generate tornadoes, hail, and gusts over a large portion of the United States in the future based on atmospheric environmental indexes (Trapp et al. 2007, 2009).

Tornadoes often occur in association with synoptic-scale extratropical cyclones (Johns et al. 1993; Niino et al. 1997), which can be reproduced by low-horizontal-resolution climate models. Lee (2012) estimated future changes of synoptic patterns favorable for tornadoes and predicted that the peak season for tornados in the United States will shift from May to April; the frequency will increase primarily between February and April but will decrease slightly between May and August. It might therefore be possible to apply synoptic climatological methods with low-horizontal-resolution climate models to project future changes in the likelihood of tornadogenesis. However, before synoptic methods can be applied to the projection of future changes, the correlation between tornadogenesis and synoptic patterns must be a priori established in the present-day climate by analyzing tornado case studies. To obtain an adequate number of tornado observations, the target areas must be enlarged, but considerably fewer tornadoes are recorded in Japan than in the United States. Furthermore, local environmental fields are strongly affected by complicated terrain such as that which characterizes the Japanese Islands. Therefore, high horizontal resolution is necessary to project future changes in conditions favoring tornadogenesis in Japan.

The archived results of a climate experiment with a 20-km-mesh atmospheric general circulation model (MRI-AGCM3.2; Mizuta et al. 2012) are very suitable for examining future changes in the occurrence possibility of strong tornadoes. The 20-km experiment

was deterministically conducted only once with the Special Report on Emission Scenarios (SRES) A1B scenario (control run), whereas an ensemble experiment with 12 members that included multiple physics and multiple sea surface temperature (SST) scenarios was also conducted to address the uncertainty of projected future changes in environmental conditions favoring tornadogenesis (Endo et al. 2012).

This is the first study to assess future changes in the occurrence of environmental conditions favorable for tornadoes in Japan using the results of the 20-km-mesh experiment. U.S. tornado statistics and the North American Regional Reanalysis (NARR) dataset (Mesinger et al. 2006) were first compared to determine the threshold values of environmental parameters for the occurrence of strong (F2 or greater on the Fujita scale) tornado events, and future changes in the United States were also investigated to verify the suitability of our analysis method by comparing future changes with those of previous studies. To verify the performance of the 20-km-mesh general circulation model, the NARR dataset was also used as a reference dataset for the present-day experiment.

This paper is organized in the following manner. In Section 2, the data, environmental parameters, and analysis method used in this study are described. Reproducibility by the numerical model of the present-day climate is described in Section 3. In Section 4, future changes in the occurrence possibility of strong tornadoes are examined. In Section 5, the results of the 20-km-horizontal-resolution model are compared with those of ensemble experiments with a horizontal resolution of 60 km. A summary and discussion are presented in the last section.

2. Methods

2.1 Climate experiment dataset

The analysis period for the present-day (future) climate was the 25-year period of 1979–2003 (2075–2099). Output from the global warming experiment was archived at intervals of 6 h (0000, 0600, 1200, and 1800 UTC) with a horizontal resolution of about 20 km (TL959) at the surface and at 16 pressure levels (975, 950, 925, 900, 850, 800, 700, 600, 500, 400, 300, 250, 200, 150, 100, and 50 hPa) in the vertical. The original model grid data were unfortunately converted to standard pressure levels, which resulted in the loss of vertical resolution near the ground, especially in high-elevation regions.

2.2 Environmental parameters

In this study, we use convective available poten-

tial energy (*CAPE*) and storm-relative environmental helicity (*SREH*) as indicators of tornadogenesis-favorable environmental conditions. *CAPE* is a metric of atmospheric instability and is calculated as follows:

$$CAPE = g \int_{Z_{LFC}}^{Z_{LNB}} \frac{T_{vp} - T_{ve}}{T_{ve}} dz \quad [J \text{ kg}^{-1}],$$

where T_{vp} and T_{ve} are virtual temperatures of a lifted air parcel and the environment, respectively, g is the acceleration of gravity, Z_{LFC} is the height of the level of free convection (*LFC*), and Z_{LNB} is the level of neutral buoyancy (*LNB*), where the virtual temperature excess first becomes zero above the *LFC*. An air parcel with the largest equivalent potential temperature in the lowest 150 hPa is lifted for calculating *CAPE*.

SREH is a measure of the tendency of a supercell to rotate, and is calculated as follows:

$$SREH = \int_0^h (\vec{V} - \vec{C}) \cdot \vec{\omega} dz \quad [m^2 \text{ s}^{-2}],$$

$$\vec{\omega} = \vec{k} \times \frac{\partial \vec{V}}{\partial z},$$

where \vec{V} is the horizontal wind vector, \vec{C} is the storm motion vector estimated from the vertical wind profile following the method of Bunkers et al. (2000), $\vec{\omega}$ is the horizontal vorticity vector associated with vertical wind shear, and the storm inflow depth h is chosen to be 3000 m AGL (above ground level).

Although high *CAPE* and *SREH* values are commonly observed near strong tornadoes, previous studies have shown that *CAPE* is not a good discriminator between a tornadogenesis-favorable environment and a non-tornadic (significant hail and wind) environment (Thompson et al. 2003; Grams et al. 2012). Environmental parameters related to low-level vertical wind shear, however, can discriminate well between the two environments. Grams et al. (2012) have shown that the 25th percentile value of the 0–1 km bulk wind difference, which is the magnitude of the vector difference between the horizontal winds at the surface and at 1 km AGL, is greater for tornado events than the median or the 75th percentile values for significant hail and wind events in the United States (See Fig. 15b in Grams et al. 2012). They have also shown that the *SREH* and the 0–1 km bulk wind difference follow the same trend. In this study, we therefore considered that conditions suitable for the occurrence of strong tornadoes can be generally discriminated with the combined use of *CAPE* and *SREH*.

2.3 Definition of threshold values for the environmental parameters

The horizontal resolution of the NARR data is about 32 km, which is coarser than that of the future climate experiments (20 km). However, the 32-km horizontal resolution of NARR could be adequate because favorable environmental fields for tornado occurrence and their corresponding index values are distributed over a distance of 40–80 km from the site of the tornado (Potvin et al. 2010). The NARR data used in this study were available every 6 h at the same times (0000, 0600, 1200, and 1800 UTC) as the climate experiment archive. The calculation of the *SREH* depends on the vertical resolution, because the vertical profile of horizontal winds in the lower troposphere exhibits rather unique characteristics when tornadoes occur (Esterheld and Giuliano 2008). Only NARR data corresponding to data levels in the climate experiment archive were therefore used to calculate *CAPE* and *SREH*. It is an additional merit of our study that the climate experiment dataset included several pressure levels at relatively low altitudes, because a tornadogenesis-favorable environment could not be properly simulated with low-vertical-resolution datasets.

Grams et al. (2012) defined a tornado event as the occurrence of one or multiple tornadoes within a 300-km radius of the occurrence site of a tornado within a timeframe of 6 h before and after its occurrence. The time and location of the event are determined from those of the tornado with the maximum Fujita Scale (F-scale) value. Figure 1 explains the procedure for defining the occurrence of tornado events and shows four examples. For the values of *CAPE* and *SREH* in the environmental field, we used the maximum values among the NARR grid points within an 80-km radius from the site of the tornado event and within 2 h before or after its occurrence.

Figure 2 presents box plots of the maximum *CAPE* and *SREH* in the environmental field for tornado events with different F-scales observed in the United States in March–April–May (MAM) and June–July–August (JJA). The values of *CAPE* indicate that the atmosphere was more unstable during relatively large F-scale tornado events and that the instability was larger in JJA than in MAM for the same F-scale. Even for F2 tornado events observed in MAM, the 25th percentile of *CAPE* reached approximately 500 J kg^{-1} . In contrast, for the same F-scale, the *SREH* was larger in MAM than in JJA. Most of the strong tornado events with F2 or stronger occurred in an environmental field with the *SREH* exceeding $150 \text{ m}^2 \text{ s}^{-2}$,

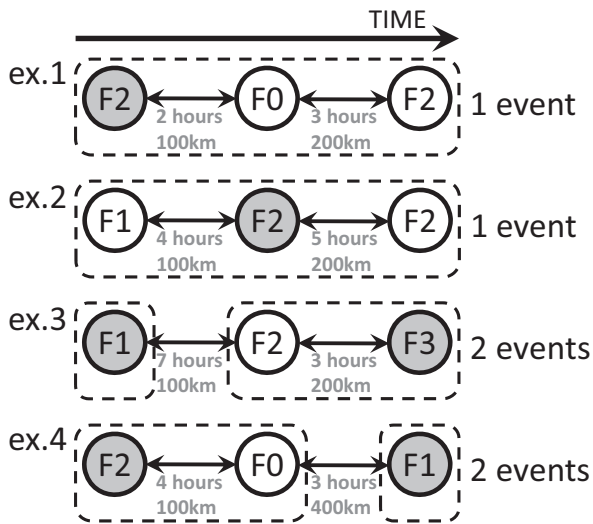


Fig. 1. Four examples of schematic diagrams for deciding whether a tornado event has occurred. A circle indicates a tornado, and tornadoes enclosed with dashed lines indicate a tornado event. The F-scale of each tornado is shown in a circle, and the occurrence time interval and distance between nearby tornadoes are indicated under the double-headed arrows. The tornadoes indicated by gray circles are the reference tornadoes for the occurrence time and site in each tornado event. The earlier tornado becomes the reference tornado if two or more tornadoes in an event have the same F-scale.

although the *SREH* was slightly smaller in JJA (25th percentile value: $129.8 \text{ m}^2 \text{ s}^{-2}$). In this study, therefore, the combination of $CAPE \geq 500 \text{ J kg}^{-1}$ and $SREH \geq 150 \text{ m}^2 \text{ s}^{-2}$ defined conditions suitable for tornadogenesis. Using these conditions, we examined the projected changes in environmental conditions favorable for tornadogenesis in MAM and JJA.

3. Reproducibility in the present-day climate

Figure 3 depicts the geographical distribution of the “appearance frequency of conditions suitable for tornadogenesis” averaged in MAM and JJA for 25 years in the present-day climate, calculated from the present-day climate experimental results and the NARR data. Hereafter, the “appearance frequency of conditions suitable for tornadogenesis” is abbreviated to FSC. The black box in Fig. 3a is “Tornado Alley,” a high-tornado-frequency area in the Great Plains (Brooks et al. 2003). In MAM (Figs. 3a, b), the FSC in the present-day climate experiment peaked

in Tornado Alley, although it was underestimated by about 25 % in the southern part. This underestimation was caused by the fact that the frequency of $CAPE \geq 500 \text{ J kg}^{-1}$ was also underestimated by approximately 20 %. In JJA (Figs. 3c, d), the present-day climate experiment successfully reproduced the geographical distribution of the FSC, especially around Tornado Alley. These results indicate that the model results can be used to project future changes in the FSC.

The fact that an area of high FSC (exceeding 10 % in Fig. 3) is distributed in Tornado Alley corresponds well with the distribution of strong tornadoes caused by supercell storms (Ashley 2007; Grams et al. 2012). In contrast, areas of low FSC ($< 2 \%$) are prevalent around the Florida peninsula, where many tornadoes also occur, though most of these are of strength F1 or F0 (Brooks et al. 2003). Around the Florida peninsula, some processes that cannot be taken into account by *CAPE* and *SREH* may contribute significantly to the occurrence of the tornadoes, because most tornadoes there occur in association with precipitation systems such as non-supercell storms or hurricanes (McCaul 1991; Smith et al. 2012). This study, therefore, focused on future changes in the occurrence of strong tornadoes (F-scale ≥ 2) such as those caused by supercell storms (i.e., supercell tornadoes).

For the Japanese region, we assumed that the same threshold values used for the United States simulations could be used to project future changes in the FSC, because no analytical data with a high horizontal resolution such as the NARR data were available for a long enough period to compare with present-day climate experimental simulations. To verify the reproducibility of the present-day climate over the Japanese region, low-level equivalent potential temperature and *SREH* were calculated in seasonal mean fields from the Japanese 55-year Reanalysis (JRA-55) (Kobayashi et al. 2015) with a grid spacing of $0.5^\circ \times 0.5^\circ$ ¹. The mean values in the present-day experiment agreed well with those in JRA-55, with the exception of the low-level equivalent potential temperature in JJA (Figs. 4, 5). The larger mean 950-hPa equivalent

¹Dataset of $0.5^\circ \times 0.5^\circ$ is produced from original data (TL319L60) with a grid spacing less than 0.5625° and 60 σ -p hybrid vertical levels as follows. The data are simply interpolated using four neighborhood points in the horizontal, and spline interpolation is applied in the vertical and 32 atmospheric pressure levels (1000, 975, 950, 925, 900, 875, 850, 825, 800, 775, 750, 700, 650, 600, 550, 500, 450, 400, 350, 300, 250, 225, 200, 175, 150, 125, 100, 70, 50, 30, 20, and 10 hPa) are prepared in addition to the surface.

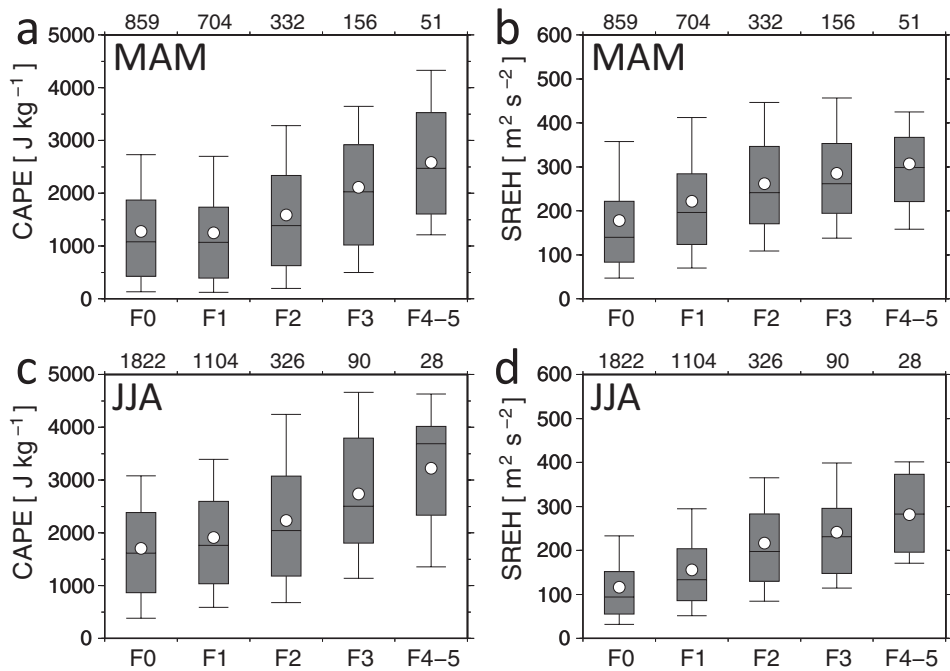


Fig. 2. Box plots of the environmental field indices for the F-scales of tornado events observed in the United States. (a) Maximum *CAPE* in MAM, (b) maximum *SREH* in MAM, (c) maximum *CAPE* in JJA, and (d) maximum *SREH* in JJA. Top (bottom) edges of boxes represent 75th (25th) percentile values. Top (bottom) whiskers represent 90th (10th) percentile values. The horizontal line within each box represents the median value. White circles indicate the mean values, and the numbers above each panel indicate the number of tornado events for each F-scale.

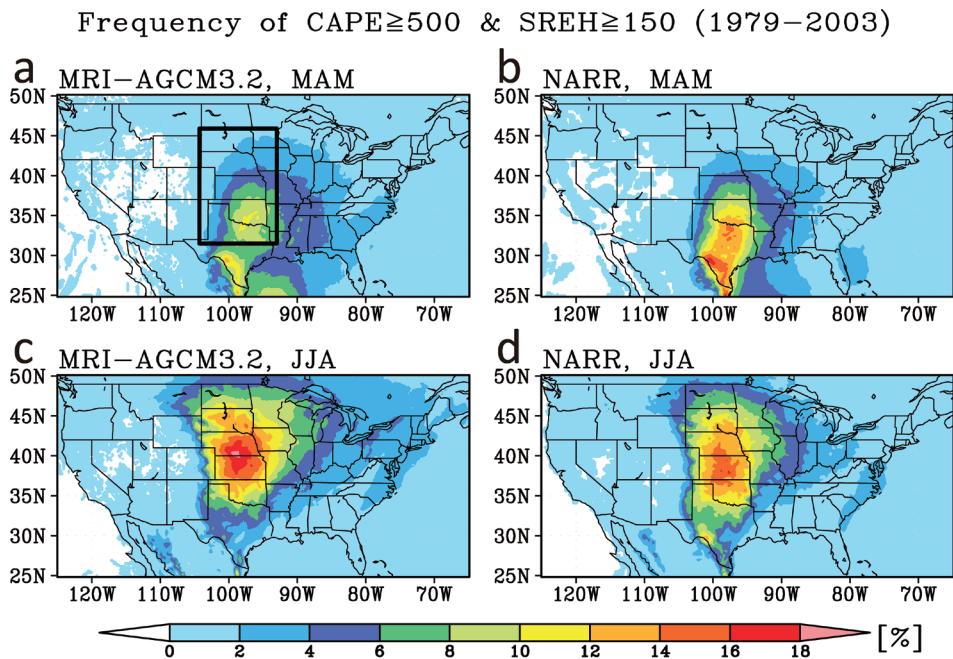


Fig. 3. Geographical distributions of the FSC in the present-day climate. (a) Present-day climate experiment in MAM, (b) NARR in MAM, (c) present-day climate experiment in JJA, and (d) NARR in JJA.

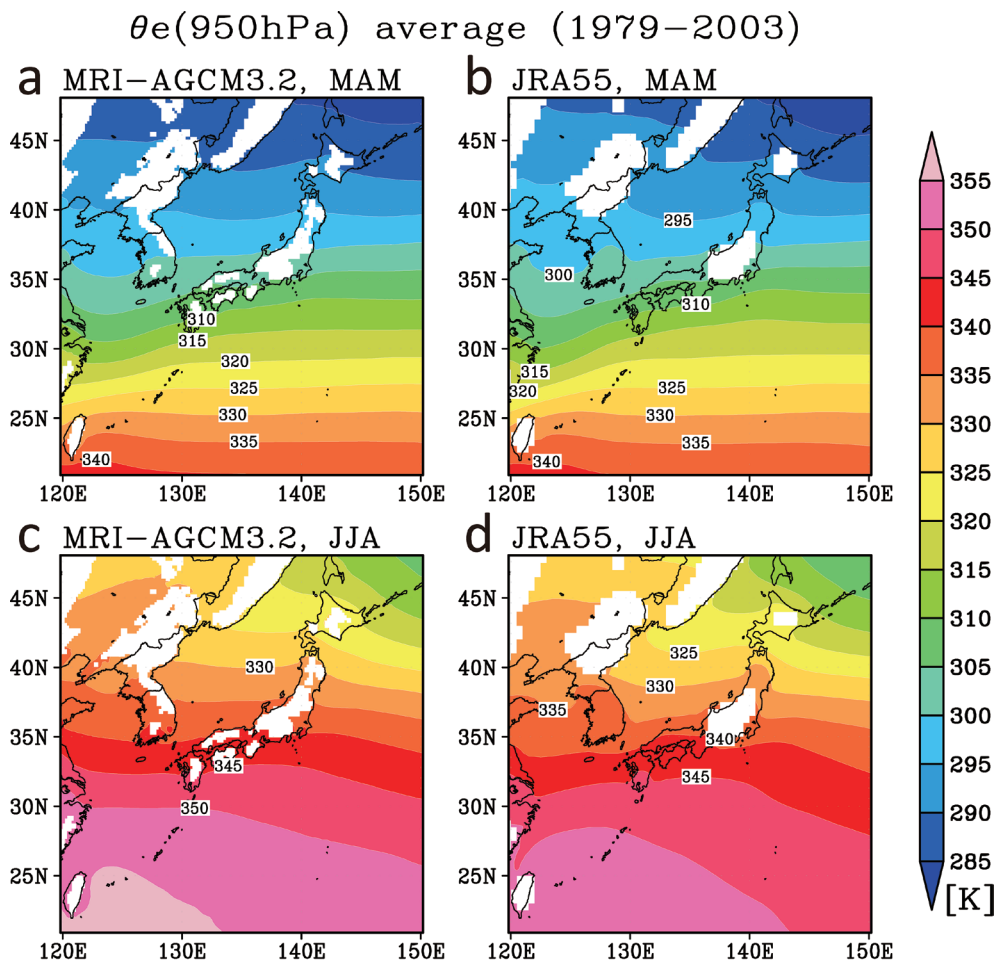


Fig. 4. Geographical distributions of equivalent potential temperature (θ_e) at 950 hPa in the present-day climate. (a) Present-day climate experiment in MAM, (b) JRA-55 in MAM, (c) present-day climate experiment in JJA, and (d) JRA-55 in JJA.

potential temperature in JJA (Figs. 4c, d) in the present-day experiment, compared with that in JRA-55, was caused by both the larger mean temperature and specific humidity at 950 hPa. In the present-day experiment, $CAPE$ was therefore overestimated in JJA, the implication being that the FSC may also have been overestimated compared to JRA-55 in JJA.

4. Future changes

4.1 The United States

Figure 6 illustrates the future/present FSC ratios in the United States in MAM and JJA based on the present-day and future climate experiments. In both seasons, the differences revealed a statistically significant increase ($p = 0.10$ based on a two-tailed t -test) of the FSC over a wide region east of 105°W (Figs.

6a, c). In particular, in Tornado Alley during MAM and JJA, the increase in the FSC reached 5 % (Figs. 6a, c). The fact that the FSC is approximately 10 % in the present-day climate (Figs. 3a, c) indicates that a future/present ratio of the FSCs exceeding 1.5 can be expected (Figs. 6b, d). The ratio of change is also large in and around the Atlantic coastal region, except for the Florida peninsula, where the future change is not statistically significant. The region with increased FSC in JJA shifts northward by about 10° compared with the analogous region in MAM (Figs. 6a, c). In MAM and JJA in the United States, the increase in the appearance frequency of $CAPE \geq 500 \text{ J kg}^{-1}$ in the future was statistically significant ($p < 0.10$) except in some regions of the Pacific Ocean coast. The increase in the appearance frequency of $CAPE \geq 500 \text{ J kg}^{-1}$

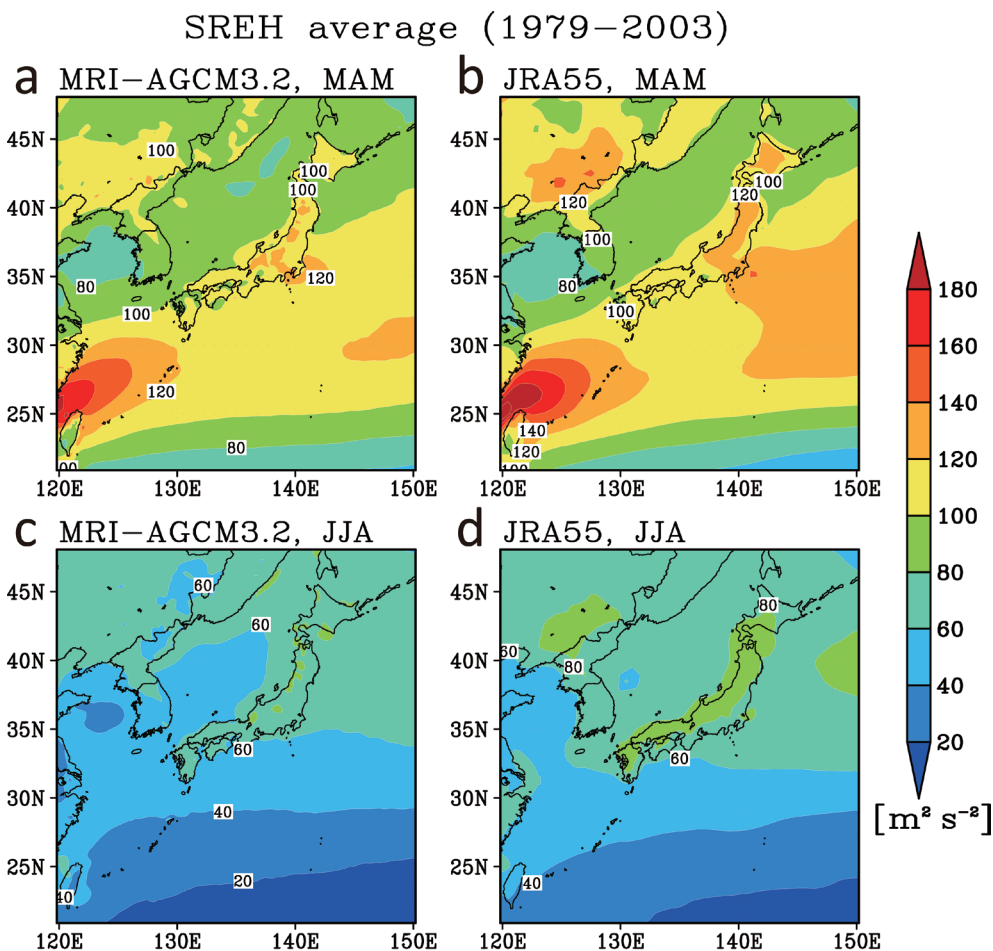


Fig. 5. Same as Fig. 4, but for *SREH*.

was caused by an increase in the water-vapor mixing ratio and temperature in the lower troposphere. In contrast, the appearance frequency of $SREH \geq 150 \text{ m}^2 \text{ s}^{-2}$ did not change significantly ($p > 0.10$) in MAM and JJA.

Previous studies based on the *SRES-A1B* scenario suggest a future increase of 20–60 % in severe thunderstorms during the warm season in Tornado Alley (Trapp et al. 2007, 2009). Another study based on the *SRES-A2* scenario projected a 20–70 % increase in tornado days over the United States between February and April (Lee 2012). Diffenbaugh et al. (2013), who projected future changes of severe thunderstorms in the United States based on the fifth phase of the Coupled Model Intercomparison Project (CMIP5), a global climate model ensemble experiment, showed an increase in the frequency of severe thunderstorms exceeding 100 % (more than twice the frequency of

the present-day climate) in Tornado Alley and the Atlantic coastal region during MAM and JJA. In contrast, according to Lee (2012) and Diffenbaugh et al. (2013), some ensemble members indicate a decrease of severe thunderstorm frequency in the southern part of Tornado Alley during JJA. However, our result for the distribution of the future/present ratios of FSCs exceeding 1.5 in tornadogenesis possibilities in Tornado Alley and the Atlantic coastal region (Fig. 6) is within the range of their projections. We therefore consider our 20-km-mesh climate experimental data and the method of analysis to be also applicable to the projection of future conditions in Japan.

4.2 Japan

In the case of Japan, the FSC was greater in JJA than in MAM in the present-day climate (Figs. 7a, d).

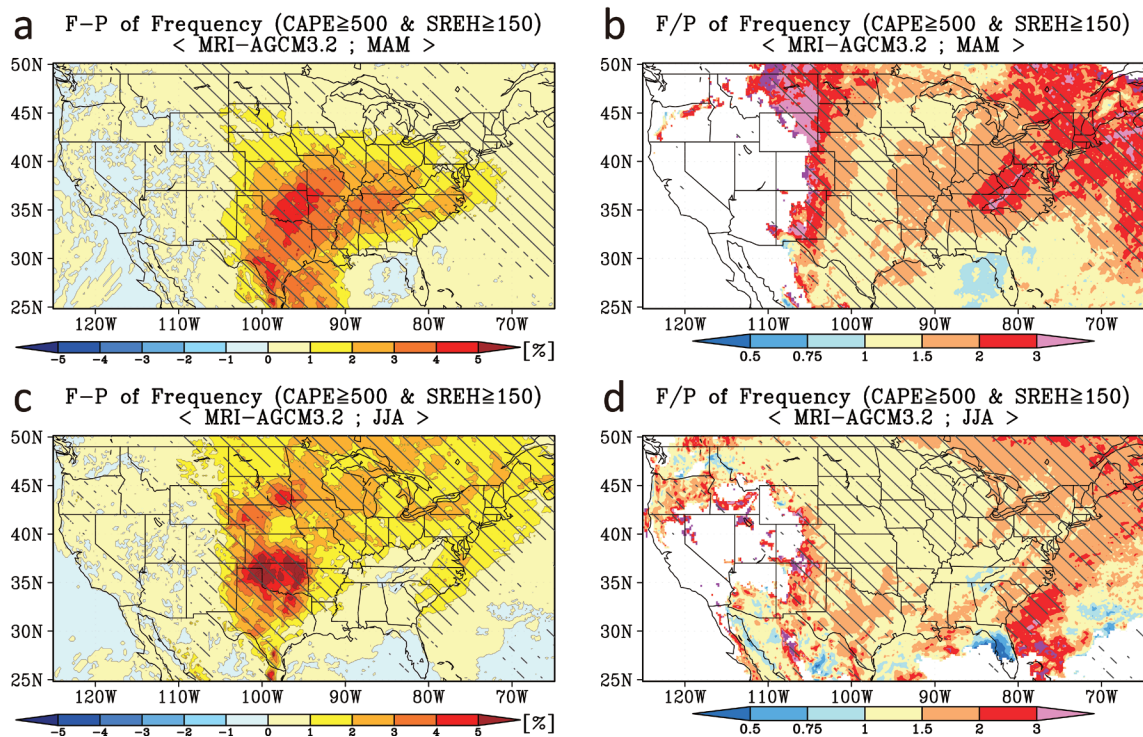


Fig. 6. Future changes in the FSC in the United States. (a) Difference (F–P) between the present-day and future climate experiments in MAM, and (c) that in JJA. (b) Change ratio (F/P) in MAM, and (d) that in JJA. Areas with a FSC less than 0.1 % in the future climate are not shaded in (c) and (d). Areas with change ratios ≥ 3.0 and a FSC less than 0.1 % in the present-day climate are shaded purple in (c) and (d). Areas where the differences of FSC between present-day and future climate are statistically significant at $p < 0.10$ by a two-tailed t -test are marked with diagonal lines.

In the future climate, we found a significant increase ($p < 0.10$) of the FSC over almost all areas of the Japanese Islands in MAM and on the Japan Sea side of the Japanese Islands in JJA (Figs. 7b, e). The difference in the FSC (Figs. 7b, e) was considerably smaller in Japan than in the United States (Figs. 6a, c), but it was comparable to the FSC in the present-day climate (Figs. 7a, d). Therefore, strong tornadoes may become twice as frequent over almost all of the Japanese Islands in MAM and on the Japan Sea side of the Japanese Islands in JJA (Figs. 7c, f).

In the future climate, the appearance frequency of $CAPE \geq 500 \text{ J kg}^{-1}$ is projected to increase significantly ($p < 0.10$) over almost all areas of the Japanese Islands in MAM and JJA (not shown). In MAM, a greater increase in FSC was found in southern Japan (Fig. 7b), whereas a high future/present ratio (> 3) of FSCs was found in western Japan and in some areas of eastern Japan (Fig. 7c). The high ratios in western and eastern Japan was calculated because in the pres-

ent-day climate the appearance frequency of $CAPE \geq 500 \text{ J kg}^{-1}$ is very low over Japan, except for southern Japan, and the appearance frequency increases in the future climate, even in northern Japan. This increase in the appearance frequency over Japan suggests that in the future climate, strong tornadoes may occur even in areas where they have never yet been observed in MAM (areas shaded purple in Fig. 7c). In JJA, a significant ($p < 0.10$) increase in high $CAPE$ conditions ($CAPE \geq 500 \text{ J kg}^{-1}$) was predicted over and around the Sea of Japan. This increase was caused mainly by the increase in sea-surface temperature over the Sea of Japan and the increase in saturated vapor pressure of the atmosphere due to the temperature rise in the lower troposphere. On the Pacific Ocean side of the Japanese Islands to the south of 35°N , the appearance frequency of $SREH \geq 150 \text{ m s}^{-2}$ decreased significantly ($p < 0.10$) in JJA. This decrease can be explained by a delay in the northward movement of the Baiu front in the future (Kusunoki

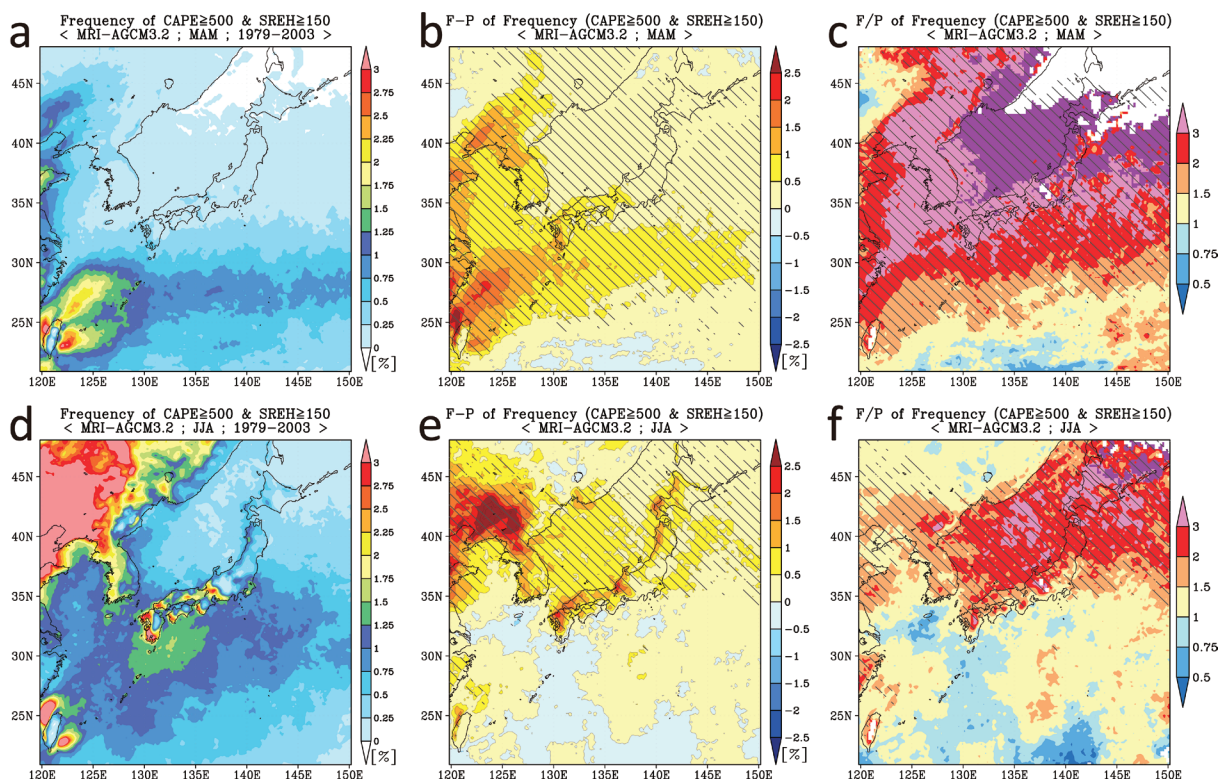


Fig. 7. Future changes in FSC in Japan. (a) Distribution of FSC in the present-day climate experiment in MAM, and (d) that in JJA. (b) Difference (F–P) between the present-day and future climate experiments in MAM, and (e) that in JJA. (c) Change ratio (F/P) in MAM, and (f) that in JJA. Areas with a FSC less than 0.1 % in the future climate are not shaded in (c) and (f). Areas with a change ratio ≥ 3.0 and a FSC less than 0.1 % in the present-day climate are shaded purple in (c) and (f). In (b), (c), (e), and (f), areas where the differences of FSC between present-day and future climate are statistically significant at $p < 0.10$ by a two-tailed t -test are marked with diagonal lines.

et al. 2006). The Baiu front is a quasi-stationary front that causes the rainy season from May to late July in East Asia.

Southerly winds composed of warm moist air typically flow into the lowest 1 km of the Baiu frontal region. Strong westerly winds occur at approximately 3-km altitude in the Baiu frontal region because the southerly winds veer clockwise with height owing to the Coriolis force when the low-level air is lifted by convective activity. The SREH tends to be larger on the south side of the Baiu front, because the southerly winds and the upper westerly winds create a large-vertical-wind-shear environment (Kato 2015).

In Japan, a considerable percentage of tornadoes is associated with typhoons that frequently approach the Japanese Islands and make landfall in autumn. Consequently, among the four seasons, tornadoes occur with maximum frequency in autumn, primarily the months

of September–October–November (SON) (Niino et al. 1997). The FSC increases slightly, even in SON in the future (Fig. 8), but the increase is not as significant as in MAM and JJA (Fig. 7). This slight increase might be caused by a decrease in the approach and landfall of typhoons in Japan, although strong typhoons are projected to increase in the future (Murakami et al. 2012b). In fact, Murakami et al. (2012b), who studied potential future changes in tropical cyclone activity by using the same 20-km-mesh climate experiment dataset as in the present study, have shown that the annual mean frequency of tropical cyclone landfalls or land approaches (within 200 km of the coast) will decrease by 35 % in the western North Pacific (see text in Murakami et al. 2012b for the domain definition). They have also shown that the annual mean instantaneous maximum surface wind speed of a tropical cyclone within 200 km of the coast of the western

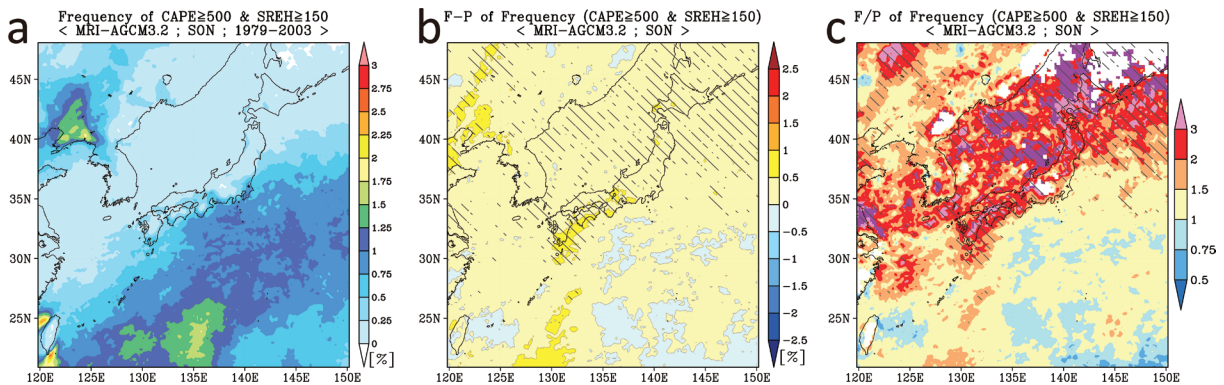


Fig. 8. Same as Fig. 7, but for SON.

North Pacific will increase by 6.5 m s^{-1} . However, additional investigations focusing on the structure of tropical cyclones, especially as they relate to tornadogenesis, will be required to project future changes of tornadoes associated with tropical cyclones.

5. Comparison with an ensemble experiment

To verify the accuracy of the projected experimental results deterministically calculated with one control run (hereafter, the deterministic experiment), an ensemble experiment was also conducted using an atmospheric general circulation model with a 60-km horizontal resolution (TL319) (Endo et al. 2012). In the ensemble experiment, three different cumulus convective parameterizations, namely the Yoshimura scheme (Yukimoto et al. 2011), the improved version of the Arakawa–Schubert scheme (Arakawa and Schubert 1974; Randall and Pan 1993), and the Kain–Fritsch scheme (Kain and Fritsch 1990, 1993) were used. Moreover, four different SSTs were specified. A total of 12 ensemble runs were therefore performed. In the deterministic experiment, only the Yoshimura scheme was used, and the SST was averaged from the predictions of 18 coupled atmosphere–ocean models that participated in the third phase of the Coupled Model Intercomparison Project (CMIP3). Based on the predictions of the coupled atmosphere–ocean models, the SSTs used in the ensemble experiment had a deviation pattern of El Niño-like SSTs, which exhibit a larger increment in the east-central tropical Pacific Ocean than in the western tropical Pacific Ocean.

Figure 9 illustrates the differences in sea-level pressure (SLP) and the 850 hPa meridional wind (V850) in the United States between the present-day and future climates in JJA. In both the deterministic and

ensemble experiments, positive anomalies of SLP were commonly found in the Gulf of Mexico and relatively lower values were found over the Great Plains (Figs. 9a, c). The anomaly pattern caused an increase in the northwest–southeast pressure gradient in the lower troposphere that intensified the V850 in a north–south direction around 100°W (Figs. 9b, d). The advection of moist, warm air associated with V850 intensification increased the appearance frequency of high *CAPE* and *SREH*, which increased the FSC in Tornado Alley in JJA (Figs. 6c, d). These common features indicate that future changes in the FSC in the deterministic experiment are highly credible. In contrast, in Tornado Alley at latitudes of $35\text{--}40^\circ\text{N}$, although all ensemble members in the 60-km experiment projected decreases in SLP, the deterministic experiment projected slight increases. The 60-km ensemble member, which involved the same experimental design as the deterministic experiment, produced results similar to the ensemble mean (Fig. 9c). This similarity may be attributable to the difference of the reproducibility of atmospheric phenomena as a function of horizontal resolution. Some of these differences were caused by terrain effects. Although some uncertainty related to model resolution exists, the common increase in V850 supports the high probability of an increase in the FSC in Tornado Alley.

Figure 10 illustrates the differences in SLP and V850 in Japan between the present-day and future climates during MAM, when the FSC is projected to increase over almost all areas of the Japanese Islands in the future (Figs. 7b, c). In the deterministic experiment and in all ensemble members, the largest negative anomaly of SLP was commonly found at the northeastern edge of the Japanese region, whereas positive anomalies were found over the ocean south of

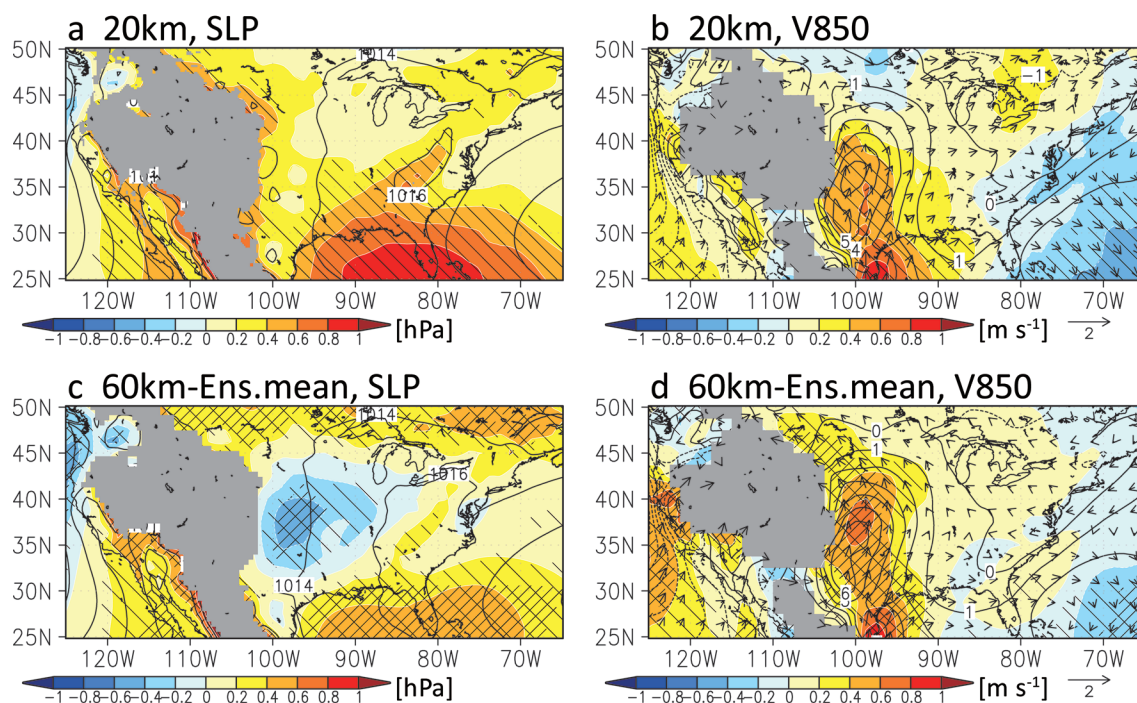


Fig. 9. Future changes in sea-level pressure (SLP) and 850-hPa meridional wind (V850) in the United States in JJA. (a) Future changes (shadings and white contours) and the present-day climate (black contours) of SLP for the 20-km model, and (b) those in V850 and 850-hPa wind (vector). (c) Same as (a), but for 60-km model ensemble experiment with 12 members, and (d) same as (b), but for the 60-km model ensemble experiment. For (a) and (b), areas where the differences were significant at $p < 0.10$ determined by a two-tailed t -test are marked with diagonal lines. For (c) and (d), areas where the sign of the future change was matched by all (more than 10) of 12 members are marked with heavy (light) diagonal lines. For (a) and (c), areas above 1000 m are masked in gray.

the Japanese Islands (Figs. 10a, c). The result that the pressure gradient force produced from this anomaly pattern intensified the southwesterly winds in western Japan can be confirmed by the V850 (Figs. 10b, d). This intensification of the southwesterly winds was consistent among all four ensemble members that used the Yoshimura scheme. This intensification and its associated advection of moist, warm air increased the frequency of high *CAPE*. These common features also support the results of the deterministic experiment.

For the United States, in both the deterministic and 11 of 12 ensemble experiments, positive anomalies in V850 were commonly projected in Tornado Alley in MAM. Furthermore, the fact that the anomalies were more pronounced in the ensemble experiment than in the deterministic experiment indicates that the FSC may increase more in Tornado Alley in MAM in the climate of the future than was predicted by the deterministic experiment (Figs. 6a, b). The ensemble

members that used the SST pattern with a slight increment of SST over the central Pacific (Cluster1 in Murakami et al. 2012a; see their Fig. 2) projected relatively large increases of V850 in Tornado Alley in MAM.

For Japan, the fact that negative anomalies in SLP extending in an east–west direction were commonly projected in JJA of both the deterministic and ensemble experiments indicates a delay in the northward movement of the Baiu front. The deterministic experiment projected V850 to intensify on the Japan Sea side of the Japanese Islands in JJA. This intensification led to an increase in *CAPE* due to the increase in low-level specific humidity. The intensification in V850 was common among all four ensemble members that used the Yoshimura scheme. In the East China Sea south of 30°N, however, most of the ensemble members that used the Kain–Fritsch scheme or the SST pattern with a large increment of SST in the tropical Western Pacific (Cluster3 in Murakami

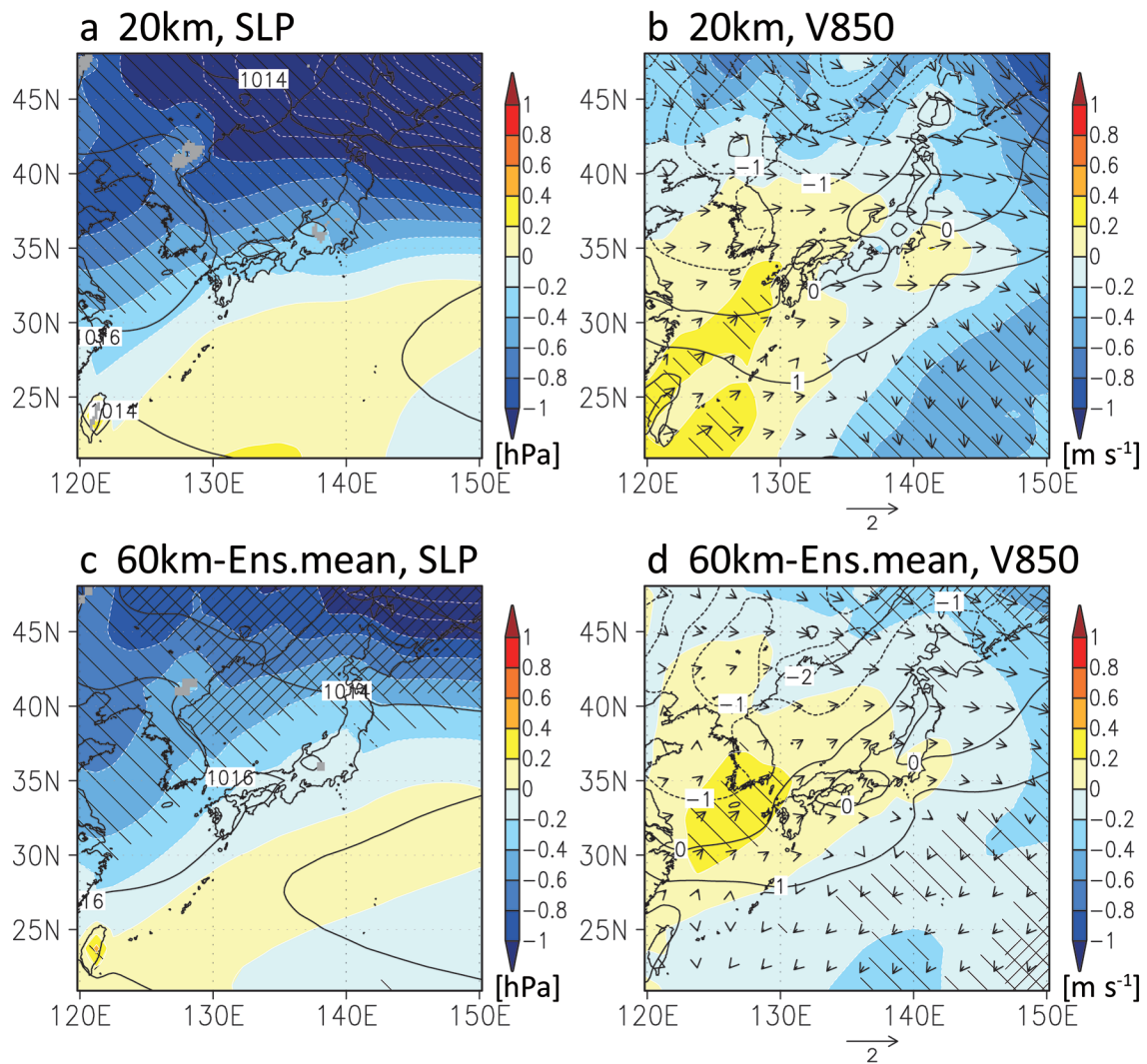


Fig. 10. Same as Fig. 9, but for the Japan region in MAM.

et. al. 2012a; see their Fig. 2) projected a decrease in V850. Negative anomalies of SLP were projected to expand further southwest by these ensemble members than by the other members, and the climatological pressure-gradient force toward the west was weakened at low levels over the East China Sea south of 30°N. The decrease in the inflow of warm, moist air due to weakening of southerly winds might depress convective activities over the Baiu front zone. Future increases of the FSC might therefore be smaller than projected by the deterministic experiment (Figs. 7e, f).

6. Summary and discussion

This study has shown that the FSC will increase in Japan between MAM and JJA. Future changes in the United States were also investigated to verify the suitability of our method of analysis by comparing the simulated future changes with those of previous studies. In the United States, the predicted distributions of the future/present ratio of FSCs (Fig. 6) were in almost all cases consistent with those of previous studies, an example being the prediction that the ratio would exceed 1.5 in Tornado Alley.

Nearly a doubling of the FSC was projected in almost all areas of the Japanese Islands in MAM and

on the Japan Sea side of the Japanese Islands in JJA. This increase was caused by a large increase in the frequency of appearance of high $CAPE$ during both time intervals, although some decrease was found to be statistically significant ($p < 0.10$) in areas of high $SREH$ in and around the Japanese Islands in JJA.

Whereas $CAPE \geq 500 \text{ J kg}^{-1}$ and $SREH \geq 150 \text{ m}^2 \text{ s}^{-2}$ were defined as suitable thresholds for the genesis of strong tornadoes in this study, they are only necessary conditions for tornadogenesis. In fact, the frequency of occurrence of $CAPE \geq 500 \text{ J kg}^{-1}$ and $SREH \geq 150 \text{ m}^2 \text{ s}^{-2}$ (Fig. 3) is much higher than that of tornadoes. This suitable condition is therefore a diagnostic guide for supercell storm generation. Moreover, previous studies have shown that only 26 % (Trapp et al. 2005) or as few as 3 % (Jones et al. 2004) of radar-detected supercell storms are accompanied by tornadoes.

In addition to $CAPE$ and $SREH$, we also investigated convective inhibition (CIN) as a predictor of tornadogenesis, because large CIN suppresses the development of moist convection. On the basis of a statistical survey of CIN when tornado events occurred in the United States (the same procedure was used in the cases of $CAPE$ and $SREH$, as described at Section 2.3), we added $30 \leq CIN \leq 400 \text{ J kg}^{-1}$ to the conditions of $CAPE \geq 500 \text{ J kg}^{-1}$ and $SREH \geq 150 \text{ m}^2 \text{ s}^{-2}$. We then estimated the future changes of these conditions. The lower threshold of CIN (30 J kg^{-1}) was the 10th percentile value, and the higher threshold (400 J kg^{-1}) was the 90th percentile value in all tornado events (not shown). The lower threshold value was applied as well, because tornado events almost never occurred when the CIN was very small, probably because low-level dry air, which reinforces downdrafts and cold outflow associated with supercell storms, is an important factor that contributes to tornadogenesis (Markowski and Richardson 2010; Noda and Niino 2010). The results showed that the characteristics of the distributions of FSC future/present ratios were very similar to those without the CIN condition (Figs. 6b, d), although FSC future/present ratios tended to increase slightly by adding the CIN condition.

In this study, future changes of tornadogenesis in Japan were estimated with the thresholds ($CAPE \geq 500 \text{ J kg}^{-1}$ and $SREH \geq 150 \text{ m}^2 \text{ s}^{-2}$) based on the statistics of U.S. tornado events (Figs. 7, 8). However, the results might differ if other suitable conditions for tornadogenesis are adopted. Moreover, it is important to verify that the threshold based on U.S. tornado events is applicable to future changes of the FSC in

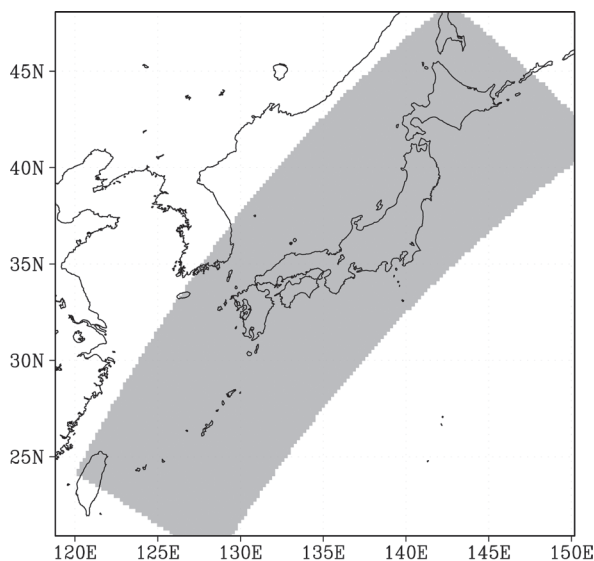


Fig. 11. The domain (shaded gray) used in the investigation with the JRA-55. The bias corrections in the appearance frequency of $CAPE$ and $SREH$ between JRA-55 and the present-day experiment were conducted in this domain.

Japan. Other thresholds of $CAPE$ and $SREH$ based on a statistical survey of tornado events (F-scale ≥ 2) that occurred in Japan from January 1961 to December 2012 were therefore examined. This survey of the Japanese region was conducted using JRA-55 with a grid spacing of $0.5^\circ \times 0.5^\circ$. Bias corrections in the appearance frequency between JRA-55 and the present-day experiment were conducted because the $0.5^\circ \times 0.5^\circ$ horizontal resolution was not enough to represent conditions suitable for tornadogenesis (Potvin et al. 2010). These procedures were as follows:

(1) The 25th percentile value of the maximum $CAPE$ ($CAPE$ -25th) when tornado events occurred was calculated with JRA-55. The definition of a tornado event was the same as that used in the United States (described in Section 2.3).

(2) The area-averaged appearance frequency of $CAPE \geq CAPE$ -25th was calculated over the area shown in Fig. 11 from January 1979 to December 2003. This area was selected to conduct bias corrections around the Japanese islands.

(3) In the present-day experiment in the same area, the threshold that produced an area-averaged appearance frequency of $CAPE$ equal to that calculated in (2) from JRA-55 was estimated.

(4) Steps (1)–(3) were also done for $SREH$.

The new suitable conditions for tornadogenesis are

Table 1. Thresholds for tornadogenesis. The values are the 25th percentile values of *CAPE* or *SREH* when tornado events occurred in Japan from January 1961 to December 2012. The revised thresholds of *CAPE* and *SREH* in each season were calculated based on the bias correction between JRA-55 and the present-day experiment using data from January 1979 to December 2003.

Parameter	Season	Threshold in JRA-55	Revised threshold for Japan
<i>CAPE</i> [J kg^{-1}]	DJF	20	30
	MAM	20	50
	JJA	250	810
	SON	190	700
<i>SREH</i> [$\text{m}^2 \text{s}^{-2}$]	DJF	130	160
	MAM	130	150
	JJA	180	190
	SON	220	270

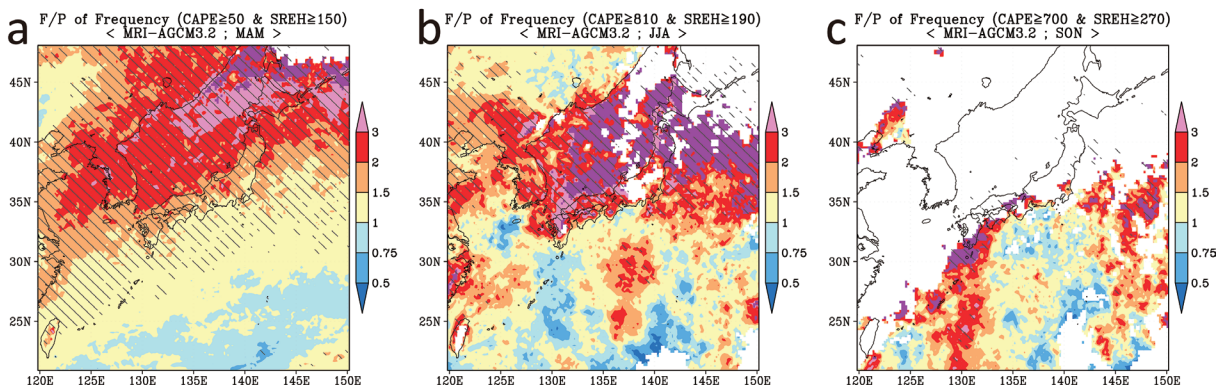


Fig. 12. As in Fig. 7c, but for future changes in FSC based on a statistical survey of tornadoes (F-scale ≥ 2) that occurred in Japan during January 1961 to December 2012. (a) Change ratio (F/P) in MAM, (b) that in JJA, and (c) that in SON. The conditions suitable for tornadogenesis were as follows: $CAPE \geq 50$ and $SREH \geq 150$ for MAM; $CAPE \geq 810$ and $SREH \geq 190$ for JJA; and $CAPE \geq 700$ and $SREH \geq 270$ for SON. Units of *CAPE* and *SREH* are J kg^{-1} and $\text{m}^2 \text{s}^{-2}$, respectively.

shown in Table 1: $CAPE \geq 50 \text{ J kg}^{-1}$ and $SREH \geq 150 \text{ m}^2 \text{s}^{-2}$ for MAM; $CAPE \geq 810 \text{ J kg}^{-1}$ and $SREH \geq 190 \text{ m}^2 \text{s}^{-2}$ for JJA; and $CAPE \geq 700 \text{ J kg}^{-1}$ and $SREH \geq 270 \text{ m}^2 \text{s}^{-2}$ for SON. In this survey with JRA-55, for December–January–February (DJF) and MAM, the 25th percentile value was calculated from 17 tornado events that occurred in both seasons (9 in DJF, 8 in MAM) because the mean differences of *CAPE* and *SREH* when tornado events occurred were not statistically significant ($p > 0.10$, two-tailed Student's *t* test) between the two seasons.

Figures 12a and 12b show that the patterns of future changes in MAM and JJA are similar to Figs. 7c and 7f, respectively, which project nearly a doubling or more over much of the area of the Japa-

nese Islands. In both time intervals, therefore, the increased occurrence of tornadoes appears to be highly robust when compared with the use of other *CAPE* and *SREH* thresholds. In SON (Fig. 12c); however, the area with a significant increase was projected to become smaller than that shown in Fig. 8c.

The present results are based on a climate experiment that was conducted deterministically with one 20-km-mesh control run; it was not an ensemble experiment with multiple runs. There is likely to be, therefore, some uncertainty in the conclusions of the present study about future changes in the environmental fields associated with the occurrence of tornadoes. Fortunately, the ensemble experiment with a

60-km resolution model supports the robustness of the deterministic projection with a 20-km model. The common projection is that there will be a significant increase in the frequency of strong tornadoes in Japan in the future.

Acknowledgments

The authors would like to express their heartfelt thanks to Dr. Tomoaki Ose of the Meteorological Research Institute of the Japan Meteorological Agency and two anonymous reviewers for their valuable comments and discussions. This work was supported by the KAKUSHIN and SOUSEI Programs of the Ministry of Education, Culture, Sports, Science, and Technology (MEXT) of Japan. The calculations were performed on the Earth Simulator. We obtained observation data of the tornadoes in the United States from the web site <http://www.spc.noaa.gov/climo/historical.html>.

References

- Arakawa, A., and W. H. Schubert, 1974: Interaction of a cumulus cloud ensemble with the large-scale environment, Part I. *J. Atmos. Sci.*, **31**, 674–701.
- Ashley, W. S., 2007: Spatial and temporal analysis of tornado fatalities in the United States: 1880–2005. *Wea. Forecasting*, **22**, 1214–1228.
- Brooks, H. E., C. A. Doswell III, and M. P. Kay, 2003: Climatological estimates of local daily tornado probability for the United States. *Wea. Forecasting*, **18**, 626–640.
- Bunkers, J. M., B. A. Klimowski, J. W. Zeitler, R. L. Thompson, and M. L. Weismann, 2000: Predicting supercell motion using a new hodograph technique. *Wea. Forecasting*, **15**, 61–79.
- Diffenbaugh, N. S., M. Scherer, and R. J. Trapp, 2013: Robust increases in severe thunderstorm environments in response to greenhouse forcing. *Proc. Natl. Acad. Sci. USA*, **110**, 16361–16366.
- Endo, H., A. Kitoh, T. Ose, R. Mizuta, and S. Kusunoki, 2012: Future changes and uncertainties in Asian precipitation simulated by multi-physics and multi-sea surface temperature ensemble experiments with high-resolution Meteorological Research Institute atmospheric general circulation models (MRI-AGCMs). *J. Geophys. Res.*, **117**, D16118, doi: 10.1029/2012JD017874.
- Esterheld, J. M., and D. J. Giuliano, 2008: Discriminating between tornadic and non-tornadic supercells: A new hodograph technique. *Electronic J. Severe Storms Meteor.*, **3**, 1–50.
- Grams, J. S., R. L. Thompson, D. V. Snively, J. A. Prentice, G. M. Hodges, and L. J. Reames, 2012: A climatology and comparison of parameters for significant tornado events in the United States. *Wea. Forecasting*, **27**, 106–123.
- Johns, R. H., J. M. Davies, and P. W. Leftwich, 1993: Some wind and instability parameters associated with strong and violent tornadoes. Part II: Variations in the combinations of wind and instability parameters. *The Tornado: Its Structure, Dynamics, Prediction, and Hazards. Geophys. Monogr.*, AGU, **79**, 583–590.
- Jones, T. A., K. M. McGrath, and J. T. Snow, 2004: Association between NSSL mesocyclone detection algorithm-detected vortices and tornadoes. *Wea. Forecasting*, **19**, 872–890.
- Kain, J. S., and J. M. Fritsch, 1990: A one-dimensional entraining/detraining plume model and its application in convective parameterization. *J. Atmos. Sci.*, **47**, 2784–2802.
- Kain, J. S., and J. M. Fritsch, 1993: Convective parameterization for mesoscale models: The Kain-Fritsch scheme. *The Representation of Cumulus Convection in Numerical Models*. Emanuel, K. A., and D. J. Raymond (eds.), Amer. Meteor. Soc., 165–170.
- Kato, T., 2015: Vertical wind shear and midlevel humidity related to formation factors on band-shaped precipitation systems. *Training Text on forecast technique*. Japan Meteorological Agency, 114–132 (in Japanese). [Available at <http://www.jma.go.jp/jma/kishou/books/yohkens/20/chapter6.pdf>.]
- Kobayashi, S., Y. Ota, Y. Harada, A. Ebata, M. Moriya, H. Onoda, K. Onogi, H. Kamahori, C. Kobayashi, H. Endo, K. Miyaoka, and K. Takahashi, 2015: The JRA-55 Reanalysis: General specifications and basic characteristics. *J. Meteor. Soc. Japan*, **93**, 5–48.
- Kusunoki, S., J. Yoshimura, H. Yoshimura, A. Noda, K. Oouchi, and R. Mizuta, 2006: Change of Baiu rain band in global warming projection by an atmospheric general circulation model with a 20-km grid size. *J. Meteor. Soc. Japan*, **84**, 581–611.
- Lee, C. C., 2012: Utilizing synoptic climatological methods to assess the impacts of climate change on future tornado-favorable environments. *Nat. Hazards*, **62**, 325–343.
- Markowski, P., and Y. Richardson, 2010: *Mesoscale Meteorology in Midlatitudes*. John Wiley & Sons, Ltd., 407 pp.
- McCaul, Jr., E. W., 1991: Buoyancy and shear characteristics of hurricane-tornado environments. *Mon. Wea. Rev.*, **119**, 1954–1978.
- Mesinger, F., G. DiMego, E. Kalnay, K. Mitchell, P. C. Shafran, W. Ebisuzaki, D. Jović, J. Woollen, E. Rogers, E. H. Berbery, M. B. Ek, Y. Fan, R. Grumbine, W. Higgins, H. Li, Y. Lin, G. Manikin, D. Parrish, and W. Shi, 2006: North American regional reanalysis. *Bull. Amer. Meteor. Soc.*, **87**, 343–360.
- Mizuta, R., H. Yoshimura, H. Murakami, M. Matsueda, H. Endo, T. Ose, K. Kamiguchi, M. Hosaka, M. Sugi, S. Yukimoto, S. Kusunoki, and A. Kitoh, 2012: Climate

- simulations using MRI-AGCM3.2 with 20-km grid. *J. Meteor. Soc. Japan*, **90A**, 233–258.
- Murakami, H., R. Mizuta, and E. Shindo, 2012a: Future changes in tropical cyclone activity projected by multi-physics and multi-SST ensemble experiments using the 60-km-mesh MRI-AGCM. *Climate Dyn.*, **39**, 2569–2584.
- Murakami, H., Y. Wang, H. Yoshimura, R. Mizuta, M. Sugi, E. Shindo, Y. Adachi, S. Yukimoto, M. Hosaka, S. Kusunoki, T. Ose, and A. Kitoh, 2012b: Future changes in tropical cyclone activity projected by the new high-resolution MRI-AGCM. *J. Climate*, **25**, 3237–3260.
- Niino, H., T. Fujitani, and N. Watanabe, 1997: A statistical study of tornadoes and waterspouts in Japan from 1961 to 1993. *J. Climate*, **10**, 1730–1752.
- Noda, A. T., and H. Niino, 2010: A numerical investigation of a supercell tornado: Genesis and vorticity budget. *J. Meteor. Soc. Japan*, **88**, 135–159.
- Potvin, C. K., K. L. Elmore, and S. J. Weiss, 2010: Assessing the impacts of proximity sounding criteria on the climatology of significant tornado environments. *Wea. Forecasting*, **25**, 921–930.
- Randall, D. A., and D.-M. Pan, 1993: Implementation of the Arakawa Schubert cumulus parameterization with a prognostic closure. *The Representation of Cumulus Convection in Numerical Models*. Emanuel, K. A., and D. J. Raymond (eds.), Amer. Meteor. Soc., 137–144.
- Rasmussen, E. N., and D. O. Blanchard, 1998: A baseline climatology of sounding-derived supercell and tornado forecast parameters. *Wea. Forecasting*, **13**, 1148–1164.
- Smith, B. T., R. L. Thompson, J. S. Grams, C. Broyles, and H. E. Brooks, 2012: Convective modes for significant severe thunderstorms in the contiguous United States. Part I: Storm classification and climatology. *Wea. Forecasting*, **27**, 1114–1135.
- Thompson, R. L., R. Edwards, J. A. Hart, K. L. Elmore, and P. Markowski, 2003: Close proximity soundings within supercell environments obtained from the Rapid Update Cycle. *Wea. Forecasting*, **18**, 1243–1261.
- Trapp, R. J., G. J. Stumpf, and K. L. Manross, 2005: A reassessment of the percentage of tornadic mesocyclones. *Wea. Forecasting*, **20**, 680–687.
- Trapp, R. J., N. S. Diffenbaugh, H. E. Brooks, M. E. Baldwin, E. D. Robinson, and J. S. Pal, 2007: Changes in severe thunderstorm environment frequency during the 21st century caused by anthropogenically enhanced global radiative forcing. *Proc. Natl. Acad. Sci. USA*, **104**, 19719–19723.
- Trapp, R. J., N. S. Diffenbaugh, and A. Gluhovsky, 2009: Transient response of severe thunderstorm forcing to elevated greenhouse gas concentrations. *Geophys. Res. Lett.*, **36**, L01703, doi:10.1029/2008GL036203.
- Yukimoto, S., H. Yoshimura, M. Hosaka, T. Sakami, H. Tsujino, M. Hirabara, T. Y. Tanaka, M. Deushi, A. Obata, H. Nakano, Y. Adachi, E. Shindo, S. Yabu, T. Ose, and A. Kitoh, 2011: Meteorological Research Institute-Earth System Model v1 (MRI-ESM1)—Model description—. *Technical Reports of Meteorological Research Institute*, **64**, 88 pp.